PHYSIOME
journal.physiomeproject.org
ISSN: 2744-6204

Energy-based bond graph models of glucose transport with SLC transporters

Weiwei Ai[1*], Peter J. Hunter[1], and David P. Nickerson[1]

[1]**Auckland Bioengineering Institute, University of Auckland, New Zealand**

ORIGINAL

Abstract

In Hunter et al. (2024), we proposed an energy-based modelling framework and presented two exemplar bond graph templates for solute carrier (SLC) transporter families: facilitated diffusion with SLC2A2 (GLUT2) and sodium-glucose cotransport with SLC5A1 (SGLT1). In this article, we provide detailed information on the parameterisation process for these two SLC families and the information required to reproduce the results presented in Hunter et al. (2024).

Keywords: SLC transporters, bond graph, energy-based modelling, CellML

Curated Model Implementation
http://doi.org/10.1037a0000000

Primary Publications

P. J. Hunter, W. Ai, and D. P. Nickerson. Energy-based bond graph models of glucose transport with slc transporters. *bioRxiv*, pages 1–24, 2024. URL https://doi.org/10.1101/2024.06.26.600892.

1 Introduction

We presented the bond graph models for the SLC2A2 and SLC5A1 solute carrier (SLC) families in Hunter et al. (2024). The models have been implemented using CellML (Cuellar et al., 2003) and the model implementation is available in the Physiome Model Repository (PMR) (Yu et al., 2011) at: https://models.physiomeproject.org/workspace/b65. In that workspace (and in the accompanying OMEX archive) the folders `Facilitated transporter` and `Electrogenic cotransporter` hold the models of SLC2A2 and SLC5A1, respectively. Brief descriptions of the CellML model files can be found in the PMR exposure: https://models.physiomeproject.org/e/b6d/. In Sections 2 & 3 we provide detailed introductions to these two exemplar models from Hunter et al. (2024). The instructions for reproducing all the simulation experiments presented in Hunter et al. (2024) are provided in Sections 2.3 & 3.3 for SLC2A2 and SLC5A1, respectively.

2 SLC2A2 bond graph model parameterisation

The SLC2A2 family (protein name GLUT2) use the extracellular to intracellular glucose concentration gradient to drive transmembrane transport in a process called 'facilitated diffusion', and we replicated the bond graph diagram in Figure 1 for convenience. The kinetic data that we used to obtain the parameters of the bond graph model were from Lowe and Walmsley (1986), while Table 1 lists the kinetic parameters. The first column of Table 1 is the corresponding parameter names for the reactions in the bond graph where the subscript indicates the reaction number, while the second column lists the kinetic parameter names in Lowe and Walmsley (1986).

OPEN ACCESS
Reproducible Model

*Corresponding author
weiwei.ai@auckland.ac.nz

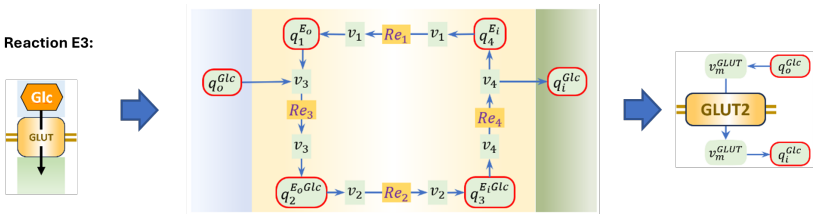

Figure 1. Bond graph of SLC2A2, replicated from Hunter et al. (2024).

Table 1. The kinetic parameters in Lowe and Walmsley (1986).

Kinetic in BG	Parameter in Lowe and Walmsley (1986)	Value	Unit
k_1	h	0.726	s^{-1}
k_2	c	1113	s^{-1}
k_3	a	4.5e7[1]	$mM^{-1}s^{-1}$
k_4	e	2.7e5 12.8459 [2]	s^{-1}
k_1	g	12.1	s^{-1}
k_2	d	90.3	s^{-1}
k_3	b	4.5e7 9.5 [3]	s^{-1}
k_4	f	2.7e5[1]	$mM^{-1}s^{-1}$

[1] Not given in Lowe and Walmsley (1986), we use a large number to align with the fast binding assumption (Lowe and Walmsley, 1986; Hunter et al., 2024).
[2] Apply the constraint $e \bullet f = 12.8459$.
[3] Apply the constraint $b \bullet a = 9.5$

2.1 Bond graph parameters

According to Pan (2019), the relationships between kinetic and bond graph parameters are captured in Equation 1.

$$\mathbf{Ln}^{1}\mathbf{k}^{o} = \mathbf{MLn}^{1}\mathbf{W}^{o} \tag{1}$$

, where

$$\mathbf{k} = \begin{bmatrix} k^{\rightarrow} \\ k \\ K^{c} \end{bmatrix}, \ \mathbf{M} = \begin{bmatrix} I_{n_r} & n_r & N^{fT} \\ I_{n_r} & n_r & N^{rT} \\ 0 & & N^{cT} \end{bmatrix}, \quad = \begin{bmatrix} K \end{bmatrix}. \tag{2}$$

The vectors of the forward and reverse kinetic rate constants $\mathbf{k}^{\rightarrow}$, $\mathbf{k}$, and the vector of known constraints K^c between the species defined in the matrix N^c are shown in Equation 3.

$$\mathbf{k}^{\rightarrow} = \begin{bmatrix} k_1^{\rightarrow} \\ k_2^{\rightarrow} \\ k_3^{\rightarrow} \\ k_4^{\rightarrow} \end{bmatrix}, \ \mathbf{k} = \begin{bmatrix} k_1 \\ k_2 \\ k_3 \\ k_4 \end{bmatrix}, \ K^c = \text{»¼}, \ \mathbf{N^c} = \text{»¼} \tag{3}$$

The order of the elements in $\mathbf{k}^{\rightarrow}$ and $\mathbf{k}$ is the same order of the reactions, organized as columns in the matrices N^f and N^r, shown in Table 2 and Table 3, while N^c is organized by [number of species] [number of K^c].

The diagonal matrix $\mathbf{W}$ (Equation 4) accounts for the volumes of compartments and the size is 10 ([number of reactions] , [number of species]). The typical blood cell volume $V_i = 0.09\ ^{1}pL^{o}$

Table 2. Forward stoichiometric matrix for the SLC 2.

	Re_1	Re_2	Re_3	Re_4
Ai	0	0	0	0
Ao	0	0	1	0
1	0	0	1	0
2	0	1	0	0
3	0	0	0	1
4	1	0	0	0

Table 3. Reverse stoichiometric matrix for the SLC 2.

	Re_1	Re_2	Re_3	Re_4
Ai	0	0	0	1
Ao	0	0	0	0
1	1	0	0	0
2	0	0	1	0
3	0	1	0	0
4	0	0	0	1

according to McLaren et al. (1987) and we set the extracellular volume $V_o = 0.09\ ^1pL^o$ as well.

$$\mathbf{W} = \begin{bmatrix} 1 & 0 & 0 & 0 & 0 & 0 & 0 & 0 & 0 & 0 \\ 0 & 1 & 0 & 0 & 0 & 0 & 0 & 0 & 0 & 0 \\ 0 & 0 & 1 & 0 & 0 & 0 & 0 & 0 & 0 & 0 \\ 0 & 0 & 0 & 1 & 0 & 0 & 0 & 0 & 0 & 0 \\ 0 & 0 & 0 & 0 & V_i & 0 & 0 & 0 & 0 & 0 \\ 0 & 0 & 0 & 0 & 0 & V_O & 0 & 0 & 0 & 0 \\ 0 & 0 & 0 & 0 & 0 & 0 & 1 & 0 & 0 & 0 \\ 0 & 0 & 0 & 0 & 0 & 0 & 0 & 1 & 0 & 0 \\ 0 & 0 & 0 & 0 & 0 & 0 & 0 & 0 & 1 & 0 \\ 0 & 0 & 0 & 0 & 0 & 0 & 0 & 0 & 0 & 1 \end{bmatrix} \tag{4}$$

Given the above vectors and matrices, we can find bond graph parameters by matrix inversion (Equation 5),

$$_0 = \mathbf{W}\ ^1\mathbf{Exp}^1\mathbf{M}\cdot\mathbf{Ln}^1\mathbf{k}^{oo} \tag{5}$$

where $\mathbf{M}$› is the Moore-Penrose pseudoinverse of $\mathbf{M}$ and $\mathbf{Exp}$ is the element-wise exponential. The resulting bond graph parameters are shown in Table 4.

2.2 Parameters for steady state

Hunter et al. (2024) provided the analytical expression (Equation 20) to calculate the parameters for the steady-state flux (Equation 19) using the bond graph parameters in Table 4. We refer the readers to the primary paper for the analytical derivation process and calculation, while we explain here how we obtained the parameters from the steady-state data (Lowe and Walmsley, 1986).

The Michaelis-Menten formulation of zero trans influx (Lowe and Walmsley, 1986) of the transporter, i.e., set the intracelluar concentration to be 0 (mM), is shown in Equation 6,

$$V_{oi} = V_{oi}^{max} \frac{»A¼_o}{K_{oi}\ ,\ »A¼_o}\ ^1mM \bullet s^o \tag{6}$$

Table 4. The bond graph parameters for SLC2A2.

Parameter	Value	Unit
K_i^A	149.65	fmol ^{1}
K_o^A	149.65	fmol ^{1}
K_1	33.2	fmol ^{1}
K_2	4.25E+03	fmol ^{1}
K_3	344.59	fmol ^{1}
K_4	1.99	fmol ^{1}
1	0.36	fmol.s ^{1}
2	0.26	fmol.s ^{1}
3	1.01E+05	fmol.s ^{1}
4	1.01E+04	fmol.s ^{1}

where $»A¼_o$ is the extracellular concentration of glucose, the maximum flux is calculated using Equation 7 with the concentration of glucose carrier molecules $»C¼$ in human red blood cells of 6.67 M (Lowe and Walmsley, 1986).

$$V_{oi}^{max} = \frac{»C¼}{1•c \ , \ 1•h} = 0.0048^{1} mM•s^{o} \tag{7}$$

The Michaelis constant of Equation 6 is calculated using Equation 8 (Lowe and Walmsley, 1986).

$$K_{oi} = \frac{b}{a}\frac{1 \ , \ g•h}{1 \ , \ c•h} = 0.1094^{1} mM^{o} \tag{8}$$

When the intracellular molar amount of glucose is zero, the steady-state expression (Equation 19 in Hunter et al. (2024)) can be rearranged to Equation 9.

$$v_{oi} = \frac{k_m^1 v_m q_o^A}{\frac{k_m^1}{K_o^A} \ , \ q_o^A} {}^{1} f\,mol•s^{o} \tag{9}$$

Substitute q_o^A in the above equation with $»A¼_o V_o$, and add the $V_E = 1^{1} pL^{o}$ term to convert the unit from ${}^{1} f\,mol•s^{o}$ to ${}^{1} mM•s^{o}$ and rearrange it to Equation 10.

$$v_{oi}^{mm} = k_m^1 v_m •V_E \frac{»A¼_o}{\frac{k_m^1}{K_o^A V_o} \ , \ »A¼_o} \tag{10}$$

We obtain the following relationships in Equations 11 and 12 by comparing Equations 6 and 10.

$$K_{io} = \frac{k_m^1}{K_o^A V_o} \tag{11}$$

$$V_{oi}^{max} = k_m^1 v_m •V_E \tag{12}$$

Hence, we obtained the parameters k_m^1 and v_m using Equations 13 and 14.

$$k_m^1 = K_{oi} K_o^A V_o = 1.4735 \tag{13}$$

$$v_m = V_{oi}^{max} \quad V_E •k_m^1 = 0.003284^{1} f\,mol•s^{o} \tag{14}$$

The Michaelis-Menten of zero trans efflux (Lowe and Walmsley, 1986) i.e., set the extracellular concentration to be 0 (mM), is shown in Equation 15.

Table 5. The parameters of the steady state for SLC2A2.

Parameter	Value	Unit
v_m	0.003284	$fmol.s^{-1}$
k_m^1	1.4735	dimensionless
k_m^2	21.671	dimensionless
k_m^3	235.07	dimensionless

$$V_{io} = V_{io}^{max} \frac{»A¼_i}{K_{io} + »A¼_i} ¹mM \bullet s^{o} \tag{15}$$

, where $»A_i¼$ is the intracelluar concentration of glucose, and the maximum flux is calculated using Equation 16.

$$V_{io}^{max} = \frac{»C¼}{1 \bullet d + 1 \bullet g} = 0.0712 ¹mM \bullet s^{o} \tag{16}$$

The Michaelis constant is calculated using Equation 17.

$$K_{io} = \frac{e}{f} \frac{1 + h \bullet g}{1 + d \bullet g} = 1.609 ¹mM^{o} \tag{17}$$

When the extracellular molar amount of glucose is zero, the steady-state expression (Equation 19 in Hunter et al. (2024)) can be rearranged to Equation 18.

$$v_{io} = \frac{k_m^2 v_m q_i^A}{\frac{k_m^2}{K_i^A} + q_i^A} ¹fmol \bullet s^{o} \tag{18}$$

Substitute q_i^A in the above equation with $»A¼_i V_i$, and add the $V_E = 1 ¹pL^{o}$ term to convert the unit from $¹fmol \bullet s^{o}$ to $¹mM \bullet s^{o}$ and rearrange it to Equation 19.

$$v_{io}^{mm} = k_m^2 v_m \bullet V_E \frac{»A¼_i}{\frac{k_m^2}{K_i^A V_i} + »A¼_i} \tag{19}$$

By comparing Equations 15 and 19, we obtained Equation 20.

$$V_{io}^{max} = k_m^2 v_m \bullet V_E \tag{20}$$

Then we can calculate the parameter k_m^2 using Equation 21.

$$k_m^2 = V_{io}^{max} \quad V_E \bullet v_m = 21.671 \tag{21}$$

k_m^3 is calculated using Equation 20 in Hunter et al. (2024). The parameters are summarized in Table 5.

2.3 Simulation results

Figure 2 shows the steady-state fluxes from the bond graph model and steady-state model (Equation 19) compared to the zero trans influx and efflux in Lowe and Walmsley (1986). The plots in red used the parameters in Table 5, while the magenta lines used the parameters calculated according to Equation 19 (Hunter et al., 2024) and the parameters in Table 4.

We summarize the models, parameters, and corresponding simulation plots in Table 6. The steady-state flux for bond graph simulation at each experimental condition is the value at $t = 250\ s$.

We have provided the Python scripts under the folder <src> to run the simulations and plot the data, while the SED-ML files in <Facilitated transporter\CellMLV2> detail the simulation settings. To get the result in Figure 2, the Python scripts *sim_GLUT2.py*, *mergeData_GLUT2.py*, *plot_GLUT2.py* should run in sequential.

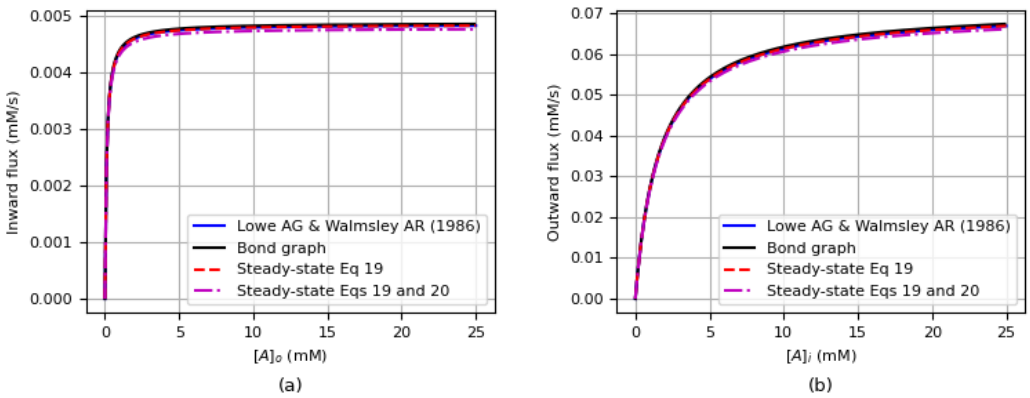

Figure 2. (a) Inward flux as a function of $»A¼_o$ when $»A¼_i = 0$, and (b) outward flux as a function of of $»A¼_i$ when $»A¼_o = 0$. Note that in order to compare with the kinetic data in Lowe and Walmsley (1986), the molar amount of glucose in the bond graph model was converted to glucose concentrations.This is Figure 8 in Hunter et al. (2024).

Table 6. Summary of the model files, parameters and corresponding simulation plots in Figure 2

Model file	Parameters	Plot in Figure 2
GLUT2_kinetic.cellml	Table 1	Lowe AG and Walmsley AR (1986) in Figure 2 (a) and (b)
GLUT2_BG.cellml	Table 4	Bond graph in Figure 2 (a) and (b)
GLUT2_ss_oi.cellml	Table 4 for Steady-state Eqs 19 and 20 and Table 5 for Steady-state Eq. 19	Steady-state Eq. 19 and Steady-state Eqs 19 and 20 in Figure 2 (a)
GLUT2_ss_io.cellml	Table 4 for Steady-state Eqs 19 and 20 and Table 5 for Steady-state Eq. 19	Steady-state Eq. 19 and Steady-state Eqs 19 and 20 in Figure 2 (b)

3 SLC5A1 bond graph model parameterization

The SLC5A1 (SGLT1) family use the sodium gradient to drive glucose into the cell, typically when the transmembrane glucose gradient is insufficient to provide the required flux of glucose. The bond graph is shown in Figure 3. We parameterize the bond graph model to fit the data in Parent et al. (1992).

The forward and reverse stoichiometric matrices (N^f, N^r) are shown in Table 7 and Table 8, respectively. The first row lists the reactions while the first column denotes the species.

The kinetic parameters in in Parent et al. (1992) are listed in Table 9. The first column is the corresponding kinetic parameters for the reactions in the bond graph where the subscript is the reaction number. The original units in Parent et al. (1992) were $mole\ ^2s\ ^1$, $mole\ ^1s\ ^1$ or $s\ ^1$, while the units were changed to $M\ ^2s\ ^1$, $M\ ^1s\ ^1$ or $s\ ^1$ in Eskandari et al. (2005) where the model (Parent et al., 1992) was reused. We found that using the units in Eskandari et al. (2005) gave the right dynamic outputs, so we used $M\ ^2s\ ^1$, $M\ ^1s\ ^1$ or $s\ ^1$ in this article and the primary paper (Hunter et al., 2024).

3.1 Bond graph parameters

We apply the same method (Pan, 2019) to convert the kinetic parameters to bond graph parameters. The vectors of the forward and reverse kinetic rate constants $k_\cdot$, $k\ $, the vector of known

Table 7. Forward stoichiometric matrix for the SLC 5.

	Re_1	Re_2	Re_3	Re_4	Re_5	Re_6	Re_7
Nai	0	0	0	0	0	0	0
Nao	2	0	0	0	0	0	0
Glci	0	0	0	0	0	0	0
Glco	0	1	0	0	0	0	0
1	1	0	0	0	0	0	0
2	0	1	0	0	0	0	1
3	0	0	1	0	0	0	0
4	0	0	0	1	0	0	0
5	0	0	0	0	1	0	0
6	0	0	0	0	0	1	0

Table 8. Reverse stoichiometric matrix for the SLC 5.

	Re_1	Re_2	Re_3	Re_4	Re_5	Re_6	Re_7
Nai	0	0	0	0	2	0	0
Nao	0	0	0	0	0	0	0
Glci	0	0	0	1	0	0	0
Glco	0	0	0	0	0	0	0
1	0	0	0	0	0	1	0
2	1	0	0	0	0	0	0
3	0	1	0	0	0	0	0
4	0	0	1	0	0	0	0
5	0	0	0	1	0	0	1
6	0	0	0	0	1	0	0

Table 9. The kinetic parameters in Fig.10 of Parent et al. (1992).

Kinetic in BG	Parameter	Value	Unit	Remark
$k_{1}^{'}$	k_{12}	80000	$M^{2}s^{1}$	$8 \quad 10^{4} \quad 10^{6}{}^{1}mM^{2}s^{1}{}^{o}$
$k_{2}^{'}$	k_{23}	1e5	$M^{1}s^{1}$	$1 \quad 10^{5} \quad 10^{3}{}^{1}mM^{1}s^{1}{}^{o}$
$k_{3}^{'}$	k_{34}	50	s^{1}	
$k_{4}^{'}$	k_{45}	800	s^{1}	
$k_{5}^{'}$	k_{56}	10	s^{1}	
$k_{6}^{'}$	k_{61}	3	s^{1}	
$k_{7}^{'}$	k_{25}	0.3	s^{1}	
k_{1}	k_{21}	500	s^{1}	
k_{2}	k_{32}	20	s^{1}	
k_{3}	k_{43}	50	s^{1}	
k_{4}	k_{54}	1.0971e7 [1]	$M^{1}s^{1}$	$1.0971e7 \quad 10^{3}{}^{1}mM^{1}s^{1}{}^{o}$
k_{5}	k_{65}	50	$M^{2}s^{1}$	$50 \quad 10^{6}{}^{1}mM^{2}s^{1}{}^{o}$
k_{6}	k_{16}	35	s^{1}	
k_{7}	k_{52}	0.823 [2]	s^{1}	

[1] k_{54} is calculated by the detailed balance equations $k_{54} = k_{23} \quad k_{34} \quad k_{45} \quad k_{52}{}^{\bullet 1}k_{32} \quad k_{43} \quad k_{25}{}^{o}$.
[2] k_{52} is calculated by the detailed balance equations $k_{52} = k_{12} \quad k_{25} \quad k_{56} \quad k_{61}{}^{\bullet 1}k_{21} \quad k_{65} \quad k_{16}{}^{o}$.

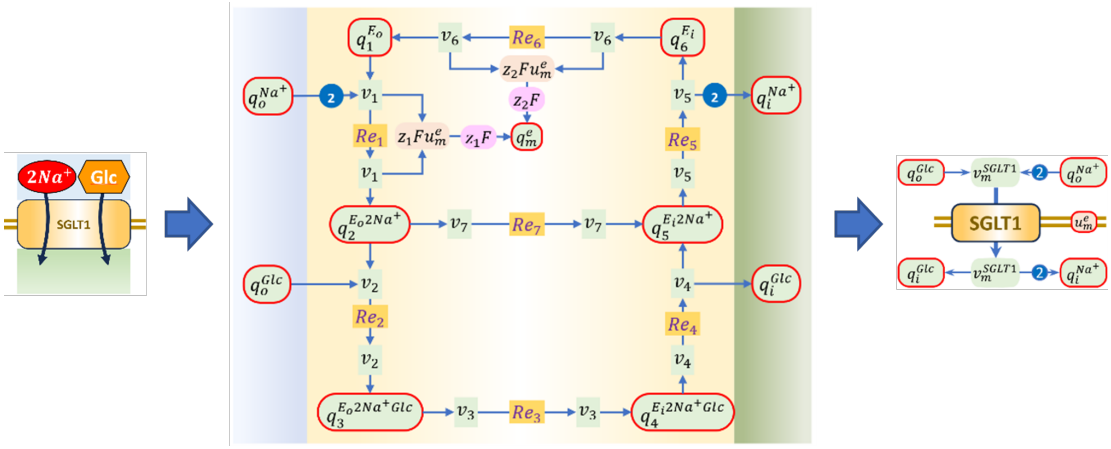

Figure 3. Bond graph of SLC5A1, replicated from Hunter et al. (2024).

constraints K^c between the species defined in the matrix N^c are:

$$\mathbf{k}^{\cdot} = \begin{bmatrix} k_1^{\cdot} \\ k_2^{\cdot} \\ k_3^{\cdot} \\ k_4^{\cdot} \\ k_5^{\cdot} \\ k_6^{\cdot} \\ k_7^{\cdot} \end{bmatrix}, \quad \mathbf{k} = \begin{bmatrix} k_1 \\ k_2 \\ k_3 \\ k_4 \\ k_5 \\ k_6 \\ k_7 \end{bmatrix}, \quad K^c = \text{»¼}, \quad \mathbf{N^c} = \text{»¼} \tag{22}$$

The blood cell volume $V_i = 8.5 \quad 10^5 pL$ in McLaren et al. (1987) and we set the extracellular volume $V_o = 8.5 \quad 10^5 pL$ as well. The diagonal matrix **W** that accounts for the volumes of compartments is constructed in Equation 23.

$$\mathbf{W} = \begin{bmatrix} 1 & 0 & 0 & 0 & 0 & 0 & 0 & 0 & 0 & 0 & 0 & 0 & 0 & 0 & 0 & 0 \\ 0 & 1 & 0 & 0 & 0 & 0 & 0 & 0 & 0 & 0 & 0 & 0 & 0 & 0 & 0 & 0 \\ 0 & 0 & 1 & 0 & 0 & 0 & 0 & 0 & 0 & 0 & 0 & 0 & 0 & 0 & 0 & 0 \\ 0 & 0 & 0 & 1 & 0 & 0 & 0 & 0 & 0 & 0 & 0 & 0 & 0 & 0 & 0 & 0 \\ 0 & 0 & 0 & 0 & 1 & 0 & 0 & 0 & 0 & 0 & 0 & 0 & 0 & 0 & 0 & 0 \\ 0 & 0 & 0 & 0 & 0 & 1 & 0 & 0 & 0 & 0 & 0 & 0 & 0 & 0 & 0 & 0 \\ 0 & 0 & 0 & 0 & 0 & 0 & 1 & 0 & 0 & 0 & 0 & 0 & 0 & 0 & 0 & 0 \\ 0 & 0 & 0 & 0 & 0 & 0 & 0 & V_i & 0 & 0 & 0 & 0 & 0 & 0 & 0 & 0 \\ 0 & 0 & 0 & 0 & 0 & 0 & 0 & 0 & V_o & 0 & 0 & 0 & 0 & 0 & 0 & 0 \\ 0 & 0 & 0 & 0 & 0 & 0 & 0 & 0 & 0 & V_i & 0 & 0 & 0 & 0 & 0 & 0 \\ 0 & 0 & 0 & 0 & 0 & 0 & 0 & 0 & 0 & 0 & V_o & 0 & 0 & 0 & 0 & 0 \\ 0 & 0 & 0 & 0 & 0 & 0 & 0 & 0 & 0 & 0 & 0 & 1 & 0 & 0 & 0 & 0 \\ 0 & 0 & 0 & 0 & 0 & 0 & 0 & 0 & 0 & 0 & 0 & 0 & 1 & 0 & 0 & 0 \\ 0 & 0 & 0 & 0 & 0 & 0 & 0 & 0 & 0 & 0 & 0 & 0 & 0 & 1 & 0 & 0 \\ 0 & 0 & 0 & 0 & 0 & 0 & 0 & 0 & 0 & 0 & 0 & 0 & 0 & 0 & 1 & 0 \\ 0 & 0 & 0 & 0 & 0 & 0 & 0 & 0 & 0 & 0 & 0 & 0 & 0 & 0 & 0 & 1 \end{bmatrix} \tag{23}$$

The bond graph parameters are shown in Table 10.

Equations 37 and 38 in Hunter et al. (2024) gave the steady-state flux under the assumption that binding and unbinding occur very rapidly in comparison with the transition rates for the carrier protein. We arbitrarily set high values of reaction rate constants to reflect the fast binding and

Table 10. The bond graph parameters for SLC5A1.

Parameter	Value	Unit
K_i^{Na}	3.22E-08	fmol ^{1}
K_o^{Na}	3.22E-08	fmol ^{1}
K_i^{Glc}	4.85E-06	fmol ^{1}
K_o^{Glc}	4.85E-06	fmol ^{1}
K_1	2.235	fmol ^{1}
K_2	10.437	fmol ^{1}
K_3	8.602	fmol ^{1}
K_4	8.602	fmol ^{1}
K_5	28.628	fmol ^{1}
K_6	0.192	fmol ^{1}
$_1$	47.905	fmol.s ^{1}
$_2$	2.325	fmol.s ^{1}
$_3$	5.812	fmol.s ^{1}
$_4$	92.998	fmol.s ^{1}
$_5$	0.349	fmol.s ^{1}
$_6$	15.661	fmol.s ^{1}
$_7$	0.029	fmol.s ^{1}

unbinding assumptions, and the parameters are shown in Table 11. Figure 4 shows the steady-state fluxes from the bond graph model and steady-state models using the parameters in Table 11, which confirms that the analytic steady-state equations 37 and 38 is a good approximation of the full bond graph model when the fast binding and unbinding assumption holds, and the slippage (reaction Re_7 in Figure 3) is negligible.

3.2 Experiment conditions

The experiment conditions in Fig. 10 of Parent et al. (1992) are shown in Table 12. A pulse protocol is applied and the holding potential is 50 mV, and at time $t = 4.75$ ms, the potential was stepped to the test potential for 80 ms. The test potentials are 50 mV and 150 mV for Fig 10, respectively. To get the I-V curve in Fig 5 (Parent et al., 1992), more test potentials are applied including 150, 120, 80, 50, 30, 0, 40, 50, 80 mV.

3.3 Simulation results

We use the parameters in Table 10 with the experiment conditions in Table 12 to simulate the time course of the carrier-mediated currents of the bond graph model under different conditions. In the bond graph model, the positive sign of $I_i = z_1 F v_1$, $z_1 F v_1$, $z_2 F v_6$, $z_2 F v_6$ with $z_1 = 0.3, z_2 = 0.7$ indicates the current from extracellular to intracelluar, while the direction of current in Parent et al. (1992) is from intracellular to extracellular. Hence, we show the model current I_i in Figure 5.

We apply a range of test potentials to the full bond graph model to produce the steady-state glucose-dependent I-V curve (red plot) shown in Figure 6. The steady-state value is derived at $t = 2.9845$s after the application of test potential at $t = 1.20475$s. The glucose-dependent current was calculated using the difference in the current value I_i at steady state before and after the addition of glucose (i.e., when » $MDG¼_o = 0$ mM and » $MDG¼_o = 1$ mM). The data from Parent et al. (1992) were derived using digitizing software Engauge Mitchell et al. (2020).

We have provided the Python scripts under the folder <src> to run the simulations and plot the data, while the SED-ML files in <Electrogenic cotransporter\CellMLV2> detail the simulation settings. To get the result in Figures 6 and 5, the Python scripts *sim_SGLT1.py*, *mergeData_SGLT1.py*, *plot_SGLT1.py* should run in sequential.

To get the steady state flux from the full bond graph SGLT1_BG_fast.cellml, we need to use

Table 11. The bond graph parameters for SLC5A1 with the fast binding/unbinding assumption.

Parameter	Value	Unit
K_i^{Na}	1.41E-07	fmol ^{1}
K_0^{Na}	1.41E-07	fmol ^{1}
K_i^{Glc}	5.72E-06	fmol ^{1}
K_0^{Glc}	5.72E-06	fmol ^{1}
K_1	3.66	fmol ^{1}
K_2	3.30E+02	fmol ^{1}
K_3	3.21E+02	fmol ^{1}
K_4	3.21E+02	fmol ^{1}
K_5	9.05E+02	fmol ^{1}
K_6	0.314	fmol ^{1}
$_1$	1.52E+04	fmol.s ^{1}
$_2$	6.24E+02	fmol.s ^{1}
$_3$	0.156	fmol.s ^{1}
$_4$	2.50E+04	fmol.s ^{1}
$_5$	1.11E+02	fmol.s ^{1}
$_6$	9.562	fmol.s ^{1}
$_7$	9.09E-04	fmol.s ^{1}

Table 12. The experiment conditions in Fig.5 and Fig. 10 of Parent et al. (1992).

Variable	Meaning	Value	Unit	Fig #	Remark
»$Na·¼_i$	Intracelluar $Na·$ concentration	20	mM	Fig.5, Fig.10	$q_i^{Na} = »Na·¼_i \quad V_i$
»$Na·¼_o$	Extracelluar $Na·$ concentration	100	mM	Fig.5, Fig.10	$q_o^{Na} = »Na·¼_o \quad V_o$
» $MDG¼_i$	Intracelluar glucose concentration	10e-3	mM	Fig.5, Fig.10	$q_i^{Glc} = »\ MDG¼_i$ V_i
» $MDG¼_o$	Extracelluar glucose concentration	0	mM	Fig.5, Fig.10 without glucose	$q_o^{Glc} = »\ MDG¼_o$ V_o
» $MDG¼_o$	Extracelluar glucose concentration	1	mM	Fig.5, Fig.10 with glucose	$q_o^{Glc} = »\ MDG¼_o$ V_o
C_T	the number of transporters per oocyte	6 10^{10}		Fig.5, Fig.10	$q_{tot} = \frac{C_T \ 10^{10}}{6.022 \ 10^{10}}$ 10^{15}
$hold_{volt}$	Holding potential	50	mV	Fig.5, Fig.10	
$test_{volt}$	Test potential	50 and 150	mV	Fig.10	More values for Fig. 5.

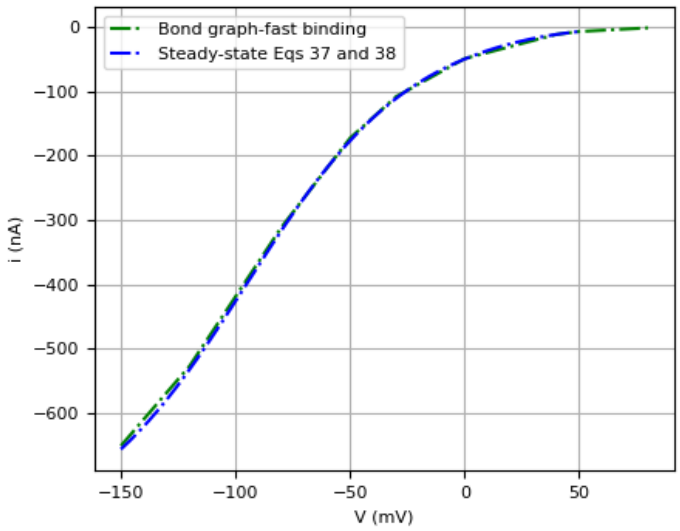

Figure 4. The steady-state results predicted by the full bond graph model, compared with the results from the reduced steady-state model. Both simulations use the assumption of fast binding/unbinding. This is Figure 10 in Hunter et al. (2024).

OpenCOR to manually run the simulation, while the SED-ML <SGLT1_BG_fast.sedml> provides the simulation settings. For each simulation, the readers need to modify the test potential (variable test_volt in params_BG_fast.cellml) to one of the values 150, 120, 80, 50, 30, 0, 40, 50, 80 mV, and the extracellular glucose concentration (variable Glco in params_BG_fast.cellml) to $1e$ 12 or 1 for before and after addition of glucose, respectively. We have provided the data in <Electrogenic cotransporter\CellMLV2\sim_results> with the filename indicating the experiment conditions. For example, SGLT1_BG_step_ss_fast_Data_sugar_m50mV.csv denotes the test potential is 50 mV and extracellular glucose concentration is 1 mM, while SGLT1_BG_step_ss_fast_Data_50mV.csv indicates the test potential is 50 mV and extracellular glucose concentration is $1e$ 12 mM (no sugar present in the filename).

4 Conclusion

We have provided here detailed information on the two exemplar models presented in Hunter et al. (2024) to demonstrate the application of the energy-based modelling framework. The derivation of the bond graph parameters has been shown and instructions on reproducing the simulation experiments presented in Hunter et al. (2024) provided. All the required model definition files and execution scripts are provided in the OMEX archive associated with this article.

References

A. A. Cuellar, C. M. Lloyd, P. F. Nielsen, D. P. Bullivant, D. P. Nickerson, and P. J. Hunter. An overview of cellml 1.1, a biological model description language. *SIMULATION*, 79(12):740–747, 2003. URL https://doi.org/10.1177/0037549703040939.

S. Eskandari, E. Wright, and D. Loo. Kinetics of the reverse mode of the na+/glucose cotransporter. *The Journal of membrane biology*, 204:23–32, 2005.

P. J. Hunter, W. Ai, and D. P. Nickerson. Energy-based bond graph models of glucose transport with slc transporters. *bioRxiv*, pages 1–24, 2024. URL https://doi.org/10.1101/2024.06.26.600892.

A. G. Lowe and A. R. Walmsley. The kinetics of glucose transport in human red blood cells. *Biochimica et Biophysica Acta (BBA)-Biomembranes*, 857(2):146–154, 1986.

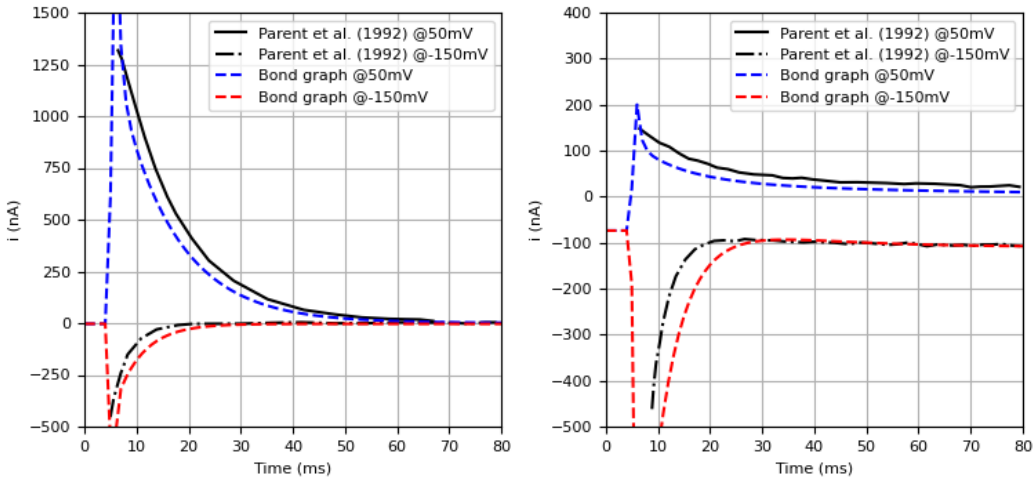

Figure 5. The time course of the carrier-mediated currents. (a) The electrical current when $»GIc¼_o = 0\,mM$ mM, and (b) the current when $»GIc¼_i = 0\,mM$; The output of the bond graph model is the current I_i, and the data of Parent et al. (1992) were derived using digitizing software Engauge (Mitchell et al., 2020) from Fig 10 (Parent et al., 1992). This is Figure 11 in Hunter et al. (2024).

C. E. McLaren, G. M. Brittenham, and V. Hasselblad. Statistical and graphical evaluation of erythrocyte volume distributions. *American Journal of Physiology-Heart and Circulatory Physiology*, 252(4):H857–H866, 1987.

M. Mitchell, B. Muftakhidinov, T. Winchen, A. Wilms, B. v. Schaik, badshah400, Mo-Gul, T. G. Badger, Z. Jędrzejewski-Szmek, kensington, and kylesower. markummitchell/engauge-digitizer: Nonrelease, July 2020. URL https://doi.org/10.5281/zenodo.3941227.

M. Pan. *A bond graph approach to integrative biophysical modelling*. PhD thesis, University of Melbourne, Parkville, Victoria, Australia, 2019.

L. Parent, S. Supplisson, D. D. Loo, and E. M. Wright. Electrogenic properties of the cloned na+/glucose cotransporter: Ii. a transport model under nonrapid equilibrium conditions. *The Journal of membrane biology*, 125:63–79, 1992.

T. Yu, C. M. Lloyd, D. P. Nickerson, M. T. Cooling, A. K. Miller, A. Garny, J. R. Terkildsen, J. Lawson, R. D. Britten, P. J. Hunter, and P. M. F. Nielsen. The Physiome Model Repository 2. *Bioinformatics*, 27(5):743–744, 01 2011. ISSN 1367-4803. URL https://doi.org/10.1093/bioinformatics/btq723.

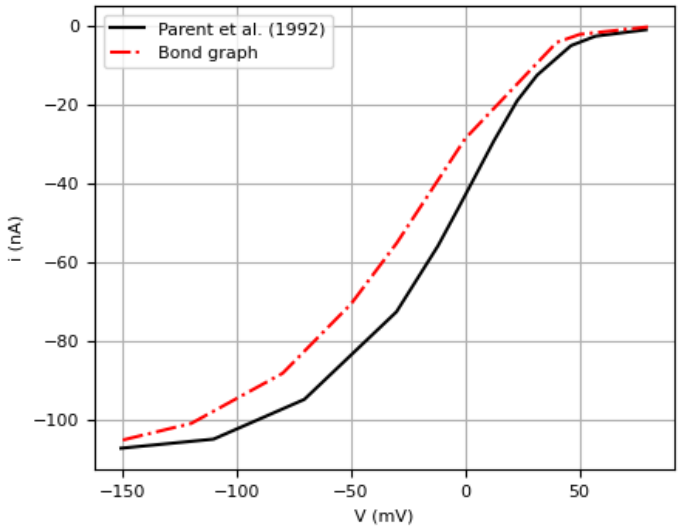

Figure 6. The full bond graph model compared with Figure 5 in Parent et al. (1992). This is Figure 12 in Hunter et al. (2024).